An investigation of the heat transfer coefficient during refrigerant evaporation

Badanie współczynnika przejmowania ciepła podczas odparowania czynnika chłodniczego

KRZYSZTOF DUTKOWSKI, MARCIN KRUZEL, TADEUSZ BOHDAL

DOI 10.36119/15.2023.10.3

This study presents the experimental research data on the local heat transfer coefficient during refrigerant expansion evaporation in horizontal pipe minichannel. Heat exchange took place between the heated channel wall and the working fluid flowing inside (R134a and R404A). AISI 316 stainless steel pipe minichannels with an internal diameter in the range of d_i = 0.64 – 2.30 mm were used. The so-called minichannels are widely used to build miniature heat exchangers. Tests carried out in the range of mass flux density G = 350 – 1400 kg/(m^2s) and heat flux density reaching q = 90 kW/m^2 allowed to observe the occurrence of the flashing phenomenon, not observed in conventional channels. It has been shown that in the zone covered by the flashing phenomenon, the heat exchange conditions deteriorate, and the value of the local heat transfer coefficient in this zone may drop by up to 50%.
Keywords: experimental data; refrigerant; heat transfer coefficient; minichannels,; expansion evaporation

W pracy przedstawiono wyniki badań eksperymentalnych lokalnego współczynnika przejmowania ciepła podczas odparowywania czynnika chłodniczego w minikanale poziomym. Wymiana ciepła odbywała się pomiędzy ogrzewaną ścianką kanału a przepływającym wewnątrz czynnikiem roboczym (R134a i R404A). Zastosowano minikanały rurowe ze stali nierdzewnej AISI 316 o średnicy wewnętrznej w zakresie d_i = 0,64 – 2,30 mm. Tak zwane minikanały są szeroko stosowane do budowy miniaturowych wymienników ciepła. Badania przeprowadzone w zakresie gęstości strumienia masy G = 350 – 1400 kg/(m^2s) i gęstości strumienia ciepła dochodzącej do q = 90 kW/m^2 pozwoliły zaobserwować występowanie zjawiska flashingu, nie obserwowanego w konwencjonalnych kanałach. Wykazano, że w strefie objętej zjawiskiem flashingu pogarszają się warunki wymiany ciepła, a wartość lokalnego współczynnika przejmowania ciepła w tej strefie może spaść nawet o 50%.
Słowa kluczowe: dane eksperymentalne; czynnik chłodniczy; współczynnik przenikania ciepła; minikanały; odparowanie rozprężne

Introduction

The term "flashing" should be understood as a phenomenon observed in a liquid when its pressure suddenly decreases and reaches a value lower than the saturation pressure at a given temperature. The liquid, which is initially in a state of thermodynamic equilibrium, turns into a superheated liquid and the process of intensive evaporation (boiling) begins inside the liquid.

Examples of the industrial application of the flashing phenomenon are: desalination processes of sea water (for the production of drinking water), drying processes, sterilization of surgical instruments. The flashing phenomenon may take place as an undesirable phenomenon, e.g. in nuclear power plants. When the reactor core cooling system fails, a high-pressure coolant is released into the environment. Then it rapidly evaporates. This is a very intensive process, which is described in the literature as a "coolant explosion"[1]. Due to the rapid phase change process, the phenomenon of expansion evaporation causes a sudden change in the temperature of the liquid. This is because the emerging vapor bubbles are heat sinks (the evaporation process requires heat, which is drawn from the immediate environment and cools it down). As a result, the temperature of the liquid begins to decrease. This ability to rapidly cool is put to practical use in some spaceflight processes, including the cooling of hot shuttle parts by spraying water under low pressure conditions [2]. Miniaturization in heat exchange devices means that the diameters of the tubes used to build the exchangers are in the order of tens or hundreds of micrometers. The flow of liquid through such channels (minichannels) is accompanied by a significant pressure drop along the route. The pressure in the line may drop locally below the saturation pressure. Then, from this cross-section, the evaporation process will start – the so-called expansion evaporation. If the expansion evaporation process takes place in the condenser, it may turn out that the condensation process is impossible to implement, because the condensed liquid undergoes expansion evaporation in the further part of the minichannel. It may happen that the expansion evaporation process takes place in the evaporator's minichannels. Then the

dr hab. inż. Krzysztof Dutkowsk; krzysztof.dutkowski@tu.koszalin.pl; https://orcid.org/0000-0003-3945-9882,
dr inż. Marcin Kruzel; marcin.kruzel@tu.koszlin.pl; https://orcid.org/0000-0001-8349-1375,
prof. dr hab. Inż. Tadeusz Bohdal; tadeusz.bohdal@tu.koszalin.pl; https://orcid.org/0000-0002-0621-2894 – Koszalin University of Technology, Faculty of Mechanical Engineering, Koszalin, Poland. Autor do korespondencji/Corresponding author: marcin.kruzel@tu.koszalin.pl

evaporation process will be driven, not as it was assumed, by the heat from the immediate environment (e.g. processor heat), but by the so-called. latent heat – heat of phase change (heat of vaporization) [3,4]. The literature revive also pointed to a certain analogy between the boiling and condensation process [5–8]. Boiling dynamics in parallel minichannel system with different inlet solutions were analyzed in [9]. Jige et al. investigated boiling heat transfer, pressure drop, and flow pattern in a horizontal square minichannel. Boiling of dispersephase droplets in a forced flow of emulsion in a minichannel was studied by Gasanov [10]. Azzolin and Bortolin [11] investigated condensation and flow boiling heat transfer of a HFO/HFC binary mixture inside a minichannel. Piasecka [12] presented miultiple correlations for flow boiling heat transfer in minichannels with various orientations. Direct local heat flux measurement during water flow boiling in a rectangular minichannel using a MEMS heat flux sensor was analyzed by Morisaki et al. [13]. Grzybowski and Masdorf [14] conducted research on dynamics of pressure drop oscillations during flow boiling inside minichannel. Feng et al. [15] presented the effects of electric field on flow boiling heat transfer in a vertical minichannel heat sink. Zhang et al. [16] used pin and wire electrodes to show the effect on flow boiling heat transfer enhancement in a vertical minichannel heat sink. See and Leong [17] studied the entropy generation for flow boiling on a single semi-circular minichannel. Experimental investigation on flow boiling was presented in [18–22]. Experimental investigations and numerical modeling of 2D temperature fields in flow boiling in minichannels were conducted by Hożejowska et al. [23]. He et al. [24] investigated flow boiling characteristics in biporous minichannel heat sink sintered with copper woven tape. Flow boiling characteristics were analyzed in [25–29]. Flow boiling of water and emulsions with a low-boiling disperse phase in minichannels were studied by Gasanov [30]. Flow boiling pressure drop and flow patterns of R-600a in a multiport minichannels were presented in [31]. Klugman et al. analyzed [32] Flow distribution and heat transfer in minigap and minichannel heat exchangers during flow boiling. Strąk et al. [33,34] investigated flow boiling heat transfer of cooling liquids in enhanced surface minichannels. The current review of the available literature indicates shortcomings in the description of the flashing phenomenon during flow boiling. A use of photographic technique for simultaneous flow boiling image recording and void fraction computation in a minichannel experiment was studied by Płaczkowski et al. [35]. Piasecka et al. [36] studied heat transfer calculations during flow in minichannels with estimation of temperature uncertainty measurements.

The paper presents the results of own research, the aim of which was to determine the impact of expansion evaporation on the intensity of the heat exchange process (heat transfer coefficient). The following refrigerants were used as the working fluid: R134a and R404A.

Experimental stand

Fig. 1 shows a diagram of the test stand. The refrigerant liquid sucked by the pump 2 from the tank 12 flowed through the filter 3 and the refrigerant pre-cooler 4. At the outflow of the liquid from the cooler, an electronic flow meter 5 (Coriolis type) was installed to measure the flow rate of the refrigerant. The liquid refrigerant was then supplied to the set of heat exchangers, which are marked in Fig. 1 with symbols 6, 7 and 8. The possibility of alternative use of these exchangers allowed to obtain the appropriate state of the refrigerant at the inlet to the test section. Thermal parameters of the refrigerant (pressure and temperature) were measured at the inlet (p_1, T_1) to the heat exchanger set and at the outlet (p_2, T_2).

Refrigerant with appropriate parameters obtained at the outflow from the set of heat exchangers (6, 7, 8) was directed to the measuring section of pipe minichannel 1. Pressure p_{in} of the refrigerant was measured in the minichannel in the inlet cross-section of the measuring section, pressure drop Δp along the length of the test section, the temperature distribution of the minichannel wall along the length of the section, the temperature of the medium at the inlet T_{in} and at the outlet from this section T_{out} and the supplied electric power P_{el}.

The refrigerant vapor leaving the measurement section 1 was supplied to the water-cooled condenser 11, and the refrigerant condensate was discharged to the tank 12 connected to the supplementary tank 13. All voltage signals of the measured quantities were supplied to the data acquisition system 18 cooperating with the computer 17.

The basic element of the test stand was the measuring section 1 containing the pipe minichannel. In the experimental studies, pipe minichannels made of stainless steel with an internal diameter of d_i = 0.45 – 2.30 mm and a total length of L = 500 mm were used. The minichannel was divided into three zones: the stabilization zone (a = 150 mm), the proper measurement section (b = 300 mm) and the outflow section (c = 50 mm). Figure 2 shows the diagram of connecting the measurement section to the test installation.

The diagram shown in Fig. 2 shows that the proper measuring section (b) was electrically heated over a length of 200 mm. The

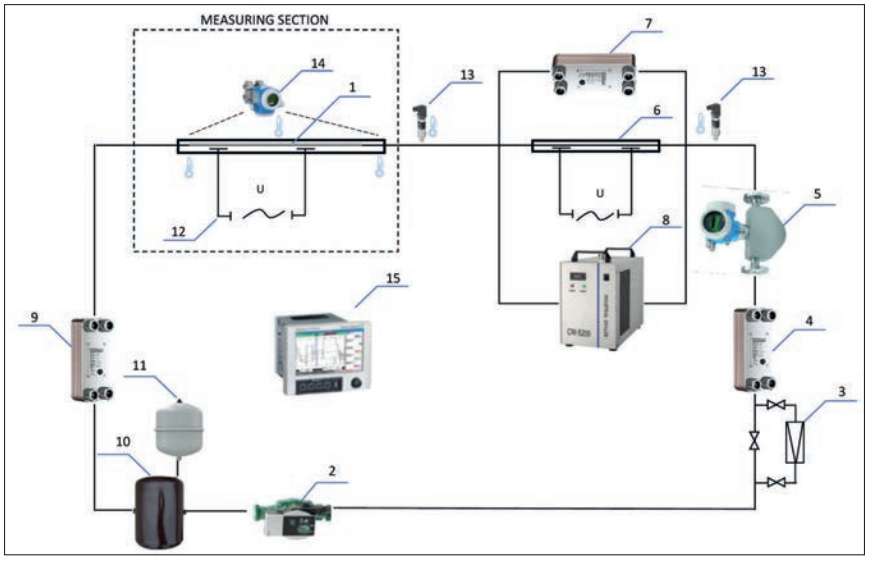

Fig. 1.
The diagram of experimental facility: 1 – pipe minichannel, 2 – pumping unit, 3 – filter, 4 – pre-cooler, 5 – flow-meter, 6 – electric heater, 7 – cooler no. 1 (cooling by tap water), 8 – refrigerating unit, 9 – condenser, 10 – liquid tank, 11 – secondary tank, 12 – electric power regulation system, 13 – pressure sensors, 16 – differential pressure sensor, 17 – data recorder
Rys. 1. Schemat stanowiska badawczego: 1 – minikanał rurowy, 2 – zespół pompowy, 3 – filtr, 4 – chłodnica wstępna, 5 – przepływomierz, 6 – nagrzewnica elektryczna, 7 – chłodnica nr. 1 (chłodzenie wodą wodociągową), 8 – agregat chłodniczy, 9 – skraplacz, 10 – zbiornik cieczy, 11 – zbiornik wtórny, 12 – układ regulacji mocy elektrycznej, 13 – czujniki ciśnienia, 16 – czujnik różnicy ciśnień, 17 – rejestrator danych

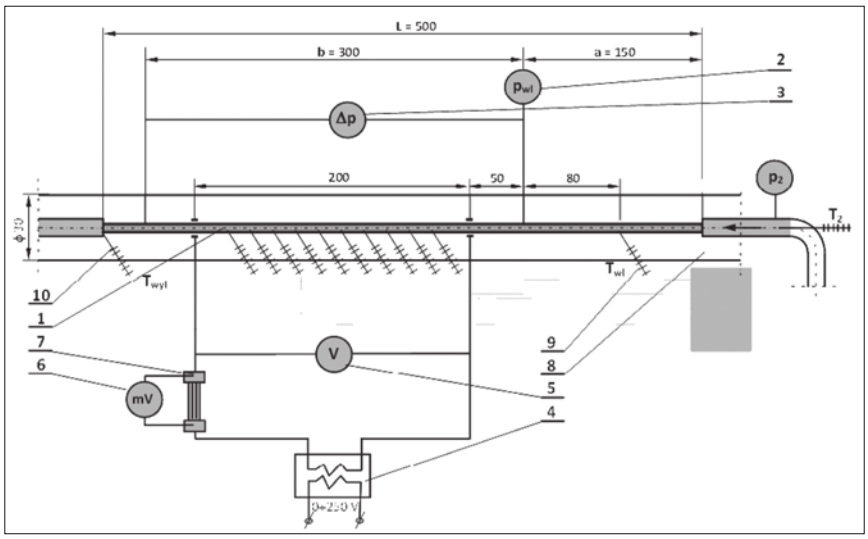

Fig. 2.
Measuring section diagram: 1 – minichannel, 2 – pressure sensor, 3 – pressure drop sensor, 4 – high-current transformer, 5 – voltmeter, 6 – millivoltmeter, 7 – high-current shunt, 8 – thermal insulation, 9 – inlet temperature, 10 – outlet temperature
Rys. 2. Schemat odcinka pomiarowego: 1 – minikanał, 2 – czujnik ciśnienia, 3 – czujnik spadku ciśnienia, 4 – przekładnik wysokoprądowy, 5 – woltomierz, 6 – miliwoltomierz, 7 – bocznik wysokoprądowy, 8 – izolacja termiczna, 9 – temperatura na wlocie, 10 – temperatura na wylocie

measuring section was included in the electric circuit.

As a result of the current flow, Joule heat was released in it. In this section, 10 sensors of K-type thermocouple thermometers were installed, evenly spaced in presections spaced 18.2 mm apart. With these sensors, the surface temperature of the outer wall of the minichannel was measured. Before the sensors were installed, their individual, experimental thermoelectric characteristics were prepared in relation to a mercury thermometer with an elementary division of 0.1 ^{0}C.

The pressure of the refrigerant at the inlet to the measuring section was measured with a piezoresistive sensor with a transducer. This sensor had a basic measurement range of 0 – 4 MPa and the measurement uncertainty resulted from its class (0.075% of the maximum indication). The pressure drop of the refrigerant over a 300 mm section of the minichannel was measured with a pressure difference sensor with a transducer with a range of 0 – 1.6 MPa (measurement uncertainty – 0.075% of the maximum indication of the device).

The measuring section as well as the pipe channels for and discharge of the refrigerant are covered with silicone insulation with an outer diameter of 36 mm.

The scope of research

Experimental studies of heat exchange were carried out during the flow in minichannels of refrigerants R134a and R404A. For each diameter of the minichannel, six measurement series were made, differing in the flow rate of the refrigerant. The value of the mass flux density G was set so as to be comparable for each diameter of the minichannel. At a fixed mass flux density, the mass flux density was increased step by step and then the heat flux density was decreased. Its maximum value did not exceed q = 90 kW/m^2. The list of the ranges of changes in the experimental parameters of the measured quantities is presented in Table 1.

Tab. 1. Range of experimental parameters
Tab. 1. Zakres zmian parametrów

d_i [mm]	G [kg/(m^{2}s)] – R134a						G [kg/(m^{2}s)] – R404A					
	I	II	III	IV	V	VI	I	II	III	IV	V	VI
0,45	380,9	427,6	551,9	808,0	961,1	1399,1	363,7	442,1	581,0	830,0	951,7	1407,8
0,55	348,3	440,8	584,0	809,6	958,0	1396,4	367,2	447,2	578,5	822,3	933,7	1401,3
0,80	361,7	436,4	568,1	811,8	953,5	1343,8	365,3	443,8	575,1	817,3	942,7	1403,8
1,10	377,4	428,4	576,2	814,1	945,1	1385,6	362,1	440,9	572,8	805,6	936,2	1400,2
1,15	360,6	449,4	583,2	820,8	956,9	1427,3	356,5	441,5	568,9	814,9	942,1	1410,2
1,30	364,6	439,4	571,1	817,0	933,5	1344,5	365,1	448,6	572,4	815,9	940,7	1399,8
1,35	364,5	438,1	566,7	809,2	938,4	1393,2	355,6	440,0	571,7	818,1	939,8	1403,1
1,40	361,3	437,1	568,7	813,3	936,3	1389,0	368,9	440,0	567,5	816,1	936,8	1394,7
1,60	365,3	438,4	557,7	816,0	941,5	1468,1	354,4	439,6	564,7	813,5	954,4	1399,4
1,68	291,6	443,8	448,3	520,5	864,2	1422,6	346,3	419,4	543,8	774,8	904,5	1333,1
1,94	355,5	441,7	567,1	813,0	945,9	1441,8	361,9	435,3	570,2	812,9	936,6	1389,1
2,30	360,7	436,7	555,9	813,6	948,5	x	363,4	441,2	576,9	790,5	944,4	x
G (average)	357,7	438,2	558,2	788,9	940,2	1401,0	360,9	440,0	570,3	811,0	938,6	1394,8

Research methodology

The local heat transfer coefficient $\alpha_{(i)}$ was calculated from the following relationship:

$$\alpha_{(i)} = \frac{q}{T_{w(i)} - T_{f(i)}}, \qquad (1)$$

where: $T_{w\,(i)}$ measured temperature of the minichannel wall in the i-th section, and q – heat flux density determined from the following relation:

$$q = \frac{Q}{A} = \frac{P_{el} - Q_{loss}}{A}, \qquad (2)$$

where the heat flux Q is the difference between the electric power delivered to the heated section of the minichannel P_{el} and the heat loss to the environment – Q_{loss}, and A the inner, heated surface of the minichannel.

Direct measurement of the refrigerant temperature ($T_{f\,(i)}$) at a cross-section $L_{(i)}$ from the inlet cross-section when flowing inside a minichannel is technically impossible. Therefore, the medium temperature values in individual sections of the measurement section were determined:

– using the heat balance method – when the pressure in section $L_{(i)}$ is greater than the saturation pressure:

$$T_{f(i)} = T_{in} + \frac{q \cdot \pi \cdot d_w \cdot L_{(i)}}{m \cdot c_p}. \qquad (3)$$

where T_{in} is the temperature of the refrigerant measured in the inlet section of the measurement section, cp – average specific heat at constant pressure of a single-phase refrigerant determined for the average refrigerant temperature;

– using tables of physical properties of the working medium, knowing that:

$$T_{f(i)} = f(p_s), \qquad (4)$$

when the pressure in section $L_{(i)}$ is lower than the saturation pressure. The value of the heat flux density (2) was calculated with an accuracy of ± 23%, while the accuracy of determining the temperature of the working medium (3) and (4) is ± 0.5K.

In sections where the local pressure of the refrigerant is less than (or equal to) the saturation pressure at a given temperature, boiling should theoretically take place. It is

known, however, that the start of the boiling process is always accompanied by a significant decrease in the wall temperature T_w. Therefore, the following cases (experimental test results) are presented below, which were obtained in the heated minichannel when bubble boiling started, causing a rapid decrease in the local wall temperature and, as follows from dependence (1), a rapid increase in the value of the local absorption coefficient heat $\alpha_{(i)}$.

Experimental data

Fig. 3 – 5 show the results of experimental tests carried out during the flow of R404A refrigerant in a heated minichannel with an internal diameter of d_i = 0.45 mm for mass flow density G = 442.1 kg/(m^{2}s). During the experiment, the phenomenon of expansion evaporation (flashing) occurred, followed by boiling, accompanied by a characteristic decrease in the wall temperature.

Figure 3 shows the distribution of the local wall temperature along the heated zone of the minichannel, obtained on the basis of measurements, for different values of the heat flux density q. The further from the beginning of the heated zone of the minichannel the measuring cross-section is located, the higher the temperature of its wall. The increase in wall temperature is the greater the greater the heat flux supplied. The proportional increase in the wall temperature along the length of the minichannel, confirmed by the rectilinear nature of the trend line, indicates (up to the value of q = 10.1 kW/m^2) a single-phase flow of the refrigerant. The boiling, which causes a rapid reduction of the wall temperature, starts at a heat flux of q = 12.1 kW/m^2 and includes cross-sections located at a distance of more than 40 mm of the heated zone of the minichannel.

Fig. 4 shows the the refrigerant temperature distribution along the length of the minichannel, calculated from dependencies (3) and (4). Already for the heat flux value q = 6.9 kW/m^2, the refrigerant in the channel core reached, in the last two sections, the saturation temperature corresponding to the local pressure. For the value of q = 10.1 kW/m^2 starting from the middle point of the minichannel the refrigerant underwent expansion evaporation, because its temperature corresponded to the saturation temperature. This fact is also confirmed by the results of the measurement of flow resistance (not presented in this paper). The start of boiling, accompanied by the passage of the boiling front, causing a rapid decrease in the wall temperature, occurred only at the heat flux density q = 12.1 kW/m^2.

The start of boiling in the flow is accompanied by a sharp increase in the intensity of the heat transfer process. It is characterized by an even several-fold increase in the value of the local heat transfer coefficient α.

Fig. 5 shows the distribution of the local heat transfer coefficient for different values of the heat flux density q. The characteristics obtained for q = 1.1 kW/m^2 and q = 3.8 kW/m^2 indicate a single-phase medium flow along the entire length of the heated

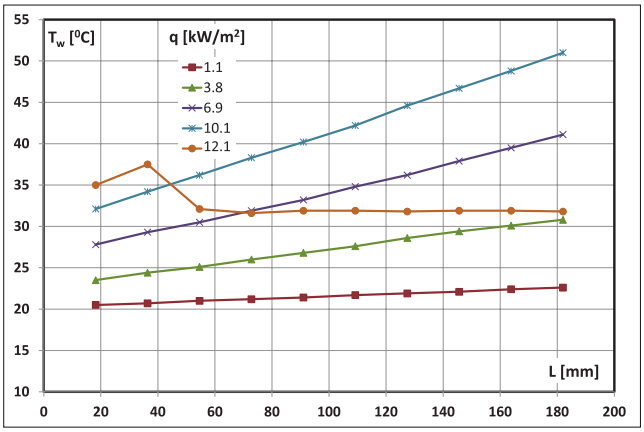

Fig. 3.
Experimental data of the channel wall temperature T_w along the minichannel length: R404A, d_i =0.45 mm, G = 442.1 kg/(m^{2}s)
Rys. 3. Dane doświadczalne temperatury ścianki kanału Tw na długości minikanału: R404A, d_i =0.45 mm, G = 442.1 kg/(m^{2}s)

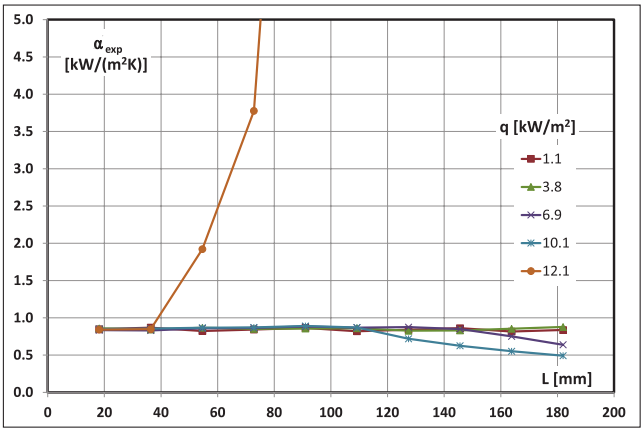

Fig. 5.
Experimental, local heat transfer coefficient along the minichannel length: R404A, d_i =0.45 mm, G = 442.1 kg/(m^{2}s)
Rys. 5. Eksperymentalne wartości lokalnego współczynnika przejmowania ciepła na długości minikanału: R404A, d_i =0.45 mm, G = 442.1 kg/(m^{2}s)

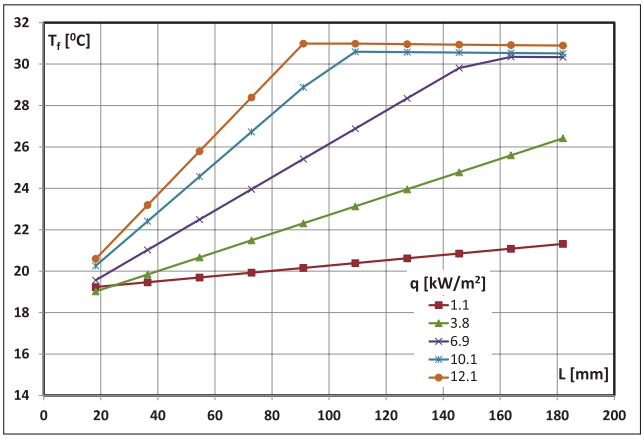

Fig. 4.
Temperature of fluid T_f along the minichannel length: R404A, d_i =0.45 mm, G = 442.1 kg/(m^{2}s)
Rys.4. Temperatura płynu T_f na długości minikanału: R404A, d_i =0.45 mm, G = 442.1 kg/(m^{2}s)

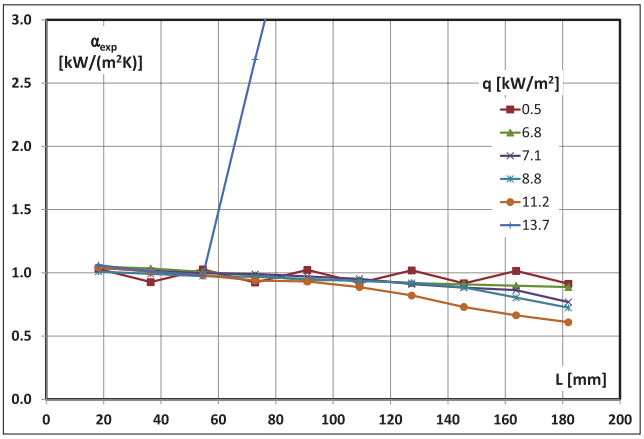

Fig. 6.
Experimental, local heat transfer coefficient along the minichannel length: R404A, d_i = 1.10 mm, G = 362.1 kg/(m^{2}s)
Rys. 6. Eksperymentalne wartości lokalnego współczynnika przejmowania ciepła na długości minikanału: R404A, d_i = 1.10 mm, G = 362.1 kg/(m^{2}s)

minichannel zone. At q = 6.9 kW/m^2, starting from the first section from the end of the heated zone of the minichannel, the value of the local coefficient decreases. Expansion evaporation has started in this zone. The resulting vapor bubbles should be treated as heat sinks, which takes latent heat from the liquid instead of the heated wall. In subsequent cases, the occurrence of expansion evaporation causes the value of the heat transfer coefficient to significantly decrease, and is even 50% lower (q = 10.1 kW/m^2 – fig. 5) than the value of the heat transfer coefficient during single-phase forced convection.

Experimental measurements, during which expansion evaporation occurred, are presented in Figures 6 – 8. These figures confirm the negative impact of the flashing phenomenon on the value of the local heat transfer coefficient.

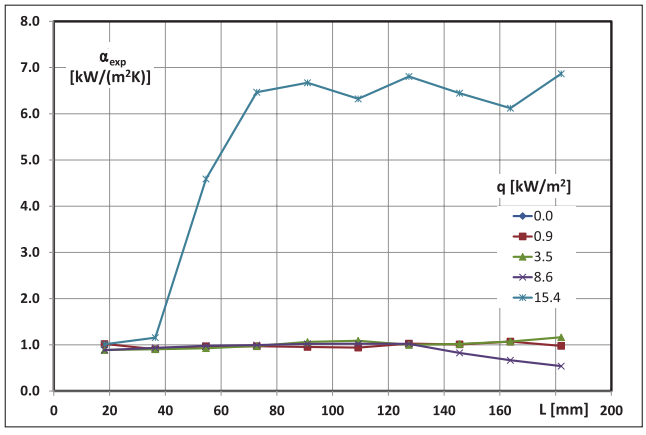

Fig. 7. Experimental, local heat transfer coefficient along the minichannel length: R134a, d_i = 0.45 mm, G = 380.9 kg/(m^{2}s)
Rys. 7. Eksperymentalne wartości lokalnego współczynnika przejmowania ciepła na długości minikanału: R134a, d_i = 0.45 mm, G = 380.9 kg/(m^{2}s)

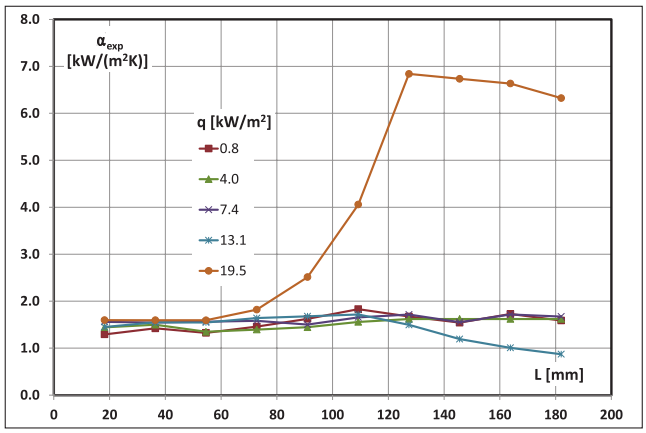

Fig. 8. Experimental, local heat transfer coefficient along the minichannel length: R134a, d_i = 0.45 mm, G = 551.9 kg/(m^{2}s)
Rys. 8. Eksperymentalne wartości lokalnego współczynnika przejmowania ciepła na długości minikanału: R134a, d_i = 0.45 mm, G = 551.9 kg/(m^{2}s)

Conclusions

Based on experimental studies carried out during the flow of R134a and R404A refrigerants in heated minichannels with an internal diameter of 0.45 – 2.30 mm, in the range of mass flow density G = 350 – 1400 kg/(m^{2}s) and flow density heat up to q = 90 kW/m^2, the following conclusions can be drawn:

1. For small values of the heat flow supplied to the refrigerant in the minichannel, heat exchange takes place by forced convection, and the process is analogous to forced convection in conventional channels.
2. During the flow of liquid in the heated minichannel, with certain thermal and flow parameters, the phenomenon of expansion evaporation may occur, the so-called evaporation. flashing not found in conventional channels.
3. The flashing phenomenon causes a significant decrease in the value of the local heat transfer coefficient in the area of its occurrence. In the tested range of parameters, the decrease in the value of the local heat transfer coefficient reached 50%.
4. Due to the decrease in the value of the local heat transfer coefficient in the area of its occurrence, the flashing phenomenon that may occur in miniature heat exchangers should be considered harmful.
5. The possibility of the flashing phenomenon should be taken into account at the design stage of devices that perform heat exchange, during the single-phase liquid flow in the minichannel.

REFERENCES

[1] Ü. Çolak, O. Özdere, Comparative analysis of pressure vessel integrity for various LOCA conditions, Journal of Nuclear Materials. 297 (2001) 271–278. https://doi.org/10.1016/S0022-3115(01)00641-9.
[2] I. Aoki, Analysis of characteristics of water flash evaporation under low-pressure conditions, Heat Transfer – Asian Research. 29 (2000) 22–33. https://doi.org/10.1002/(sici)1523-1496(200001)29:1<22::aid-htj3>3.0.co;2-v.
[3] D. Saury, S. Harmand, M. Siroux, Experimental study of flash evaporation of a water film, n.d. www.elsevier.com/locate/ijhmt.
[4] D. Saury, S. Harmand, M. Siroux, Flash evaporation from a water pool: Influence of the liquid height and of the depressurization rate, International Journal of Thermal Sciences. 44 (2005) 953–965. https://doi.org/10.1016/j.ijthermalsci.2005.03.005.
[5] M. Kruzel, T. Bohdal, K. Dutkowski, W. Kuczy, Current Research Trends in the Process of Condensation of Cooling Zeotropic Mixtures in Compact Condensers, (2022).
[6] T. Bohdal, H. Charun, M. Kruzel, M. Sikora, High pressure refrigerants condensation in vertical pipe minichannels, Int J Heat Mass Transf. (2019). https://doi.org/10.1016/j.ijheatmasstransfer.2019.02.037.
[7] T. Bohdal, H. Charun, M. Kruzel, M. Sikora, An investigation of heat transfer coefficient during refrigerants condensation in vertical pipe minichannels, in: E3S Web of Conferences, 2018. https://doi.org/10.1051/e3sconf/20187002001.
[8] K. Dutkowski, Air–Water Two-Phase Frictional Pressure Drop in Minichannels, Heat Transfer Engineering. 31 (2010) 321–330. https://doi.org/10.1080/01457630903312080.
[9] I. Zaborowska, H. Grzybowski, G. Rafałko, R. Mosdorf, Boiling dynamics in parallel minichannel system with different inlet solutions, Int J Heat Mass Transf. 165 (2021). https://doi.org/10.1016/j.ijheatmasstransfer.2020.120655.
[10] B.M. Gasanov, Boiling of disperse-phase droplets in a forced flow of emulsion in a minichannel, Int J Heat Mass Transf. 142 (2019). https://doi.org/10.1016/j.ijheatmasstransfer.2019.118454.
[11] M. Azzolin, S. Bortolin, Condensation and flow boiling heat transfer of a HFO/HFC binary mixture inside a minichannel, International Journal of Thermal Sciences. 159 (2021). https://doi.org/10.1016/j.ijthermalsci.2020.106638.
[12] M. Piasecka, Correlations for flow boiling heat transfer in minichannels with various orientations, Int J Heat Mass Transf. 81 (2015) 114–121. https://doi.org/10.1016/j.ijheatmasstransfer.2014.09.063.
[13] M. Morisaki, S. Minami, K. Miyazaki, T. Yabuki, Direct local heat flux measurement during water flow boiling in a rectangular minichannel using a MEMS heat flux sensor, Exp Therm Fluid Sci. 121 (2021). https://doi.org/10.1016/j.expthermflusci.2020.110285.
[14] H. Grzybowski, R. Mosdorf, Dynamics of pressure drop oscillations during flow boiling inside minichannel, International Communications in Heat and Mass Transfer. 95 (2018) 25–32. https://doi.org/10.1016/j.icheatmasstransfer.2018.03.025.
[15] Z. Feng, X. Luo, J. Zhang, J. Xiao, W. Yuan, Effects of electric field on flow boiling heat transfer in a vertical minichannel heat sink, Int J Heat Mass Transf. 124 (2018) 726–741. https://doi.org/10.1016/j.ijheatmasstransfer.2018.03.067.
[16] J. Zhang, X. Luo, Z. Feng, F. Guo, Effects of pin and wire electrodes on flow boiling heat transfer enhancement in a vertical minichan-

nel heat sink, Int J Heat Mass Transf. 136 (2019) 740–754. https://doi.org/10.1016/j.ijheatmasstransfer.2019.03.043.
[17] Y.S. See, K.C. Leong, Entropy generation for flow boiling on a single semi-circular minichannel, Int J Heat Mass Transf. 154 (2020). https://doi.org/10.1016/j.ijheatmasstransfer.2020.119689.
[18] Y. Lan, Z. Feng, Z. Hu, S. Zheng, J. Zhou, Y. Zhang, Z. Huang, J. Zhang, W. Lu, Experimental investigation on the effects of swirling flow on flow boiling heat transfer and instability in a minichannel heat sink, Appl Therm Eng. 219 (2023). https://doi.org/10.1016/j.applthermaleng.2022.119512.
[19] B. Markal, A. Candan, O. Aydin, M. Avci, Experimental investigation of flow boiling in single minichannels with low mass velocities, International Communications in Heat and Mass Transfer. 98 (2018) 22–30. https://doi.org/10.1016/j.icheatmasstransfer.2018.08.002.
[20] F. Yu, X. Luo, B. He, J. Xiao, W. Wang, J. Zhang, Experimental investigation of flow boiling heat transfer enhancement under ultrasound fields in a minichannel heat sink, Ultrason Sonochem. 70 (2021). https://doi.org/10.1016/j.ultsonch.2020.105342.
[21] J. Xiao, J. Zhang, Experimental investigation on flow boiling bubble motion under ultrasonic field in vertical minichannel by using bubble tracking algorithm, Ultrason Sonochem. 95 (2023) 106365. https://doi.org/10.1016/j.ultsonch.2023.106365.
[22] S. Hong, C. Dang, E. Hihara, Experimental investigation on flow boiling characteristics of radial expanding minichannel heat sinks applied for two-phase flow inlet, Int J Heat Mass Transf. 151 (2020). https://doi.org/10.1016/j.ijheatmasstransfer.2020.119316.
[23] S. Hożejowska, R.M. Kaniowski, M.E. Poniewski, Experimental investigations and numerical modeling of 2D temperature fields in flow boiling in minichannels, Exp Therm Fluid Sci. 78 (2016) 18–29. https://doi.org/10.1016/j.expthermflusci.2016.05.005.
[24] B. He, P. /Dr X. Luo, F. Yu, J. Zhou, J. Zhang, Flow boiling characteristics in bi-porous minichannel heat sink sintered with copper woven tape, Int J Heat Mass Transf. 158 (2020). https://doi.org/10.1016/j.ijheatmasstransfer.2020.119988.
[25] L. Wang, X. Luo, J. Zhang, B. He, Z. Peng, Flow boiling characteristics of minichannel heat sink with artificial conical cavities array under electric field, Int J Heat Mass Transf. 173 (2021). https://doi.org/10.1016/j.ijheatmasstransfer.2021.121286.
[26] Y. Sun, L. Zhang, H. Xu, X. Zhong, Flow boiling enhancement of FC-72 from microporous surfaces in minichannels, Exp Therm Fluid Sci. 35 (2011) 1418–1426. https://doi.org/10.1016/j.expthermflusci.2011.05.010.
[27] J. Zhou, X. Luo, Y. Pan, D. Wang, J. Xiao, J. Zhang, B. He, Flow boiling heat transfer coefficient and pressure drop in minichannels with artificial activation cavities by direct metal laser sintering, Appl Therm Eng. 160 (2019). https://doi.org/10.1016/j.applthermaleng.2019.113837.
[28] J. Zhou, X. Luo, C. Li, L. Liang, G. Wang, B. He, Z.Q. Tian, Flow boiling heat transfer enhancement under ultrasound field in minichannel heat sinks, Ultrason Sonochem. 78 (2021). https://doi.org/10.1016/j.ultsonch.2021.105737.
[29] A. Ateş, S. Çelik, V. Yağcı, M. Çağlar Malyemez, M. Parlak, A.K. Sadaghiani, A. Koşar, Flow boiling of dielectric fluid HFE – 7000 in a minichannel with pin fin structured surfaces, Appl Therm Eng. 223 (2023). https://doi.org/10.1016/j.applthermaleng.2023.120045.
[30] B.M. Gasanov, Flow boiling of water and emulsions with a low-boiling disperse phase in minichannels, Int J Heat Mass Transf. 126 (2018) 9–14. https://doi.org/10.1016/j.ijheatmasstransfer.2018.05.143.
[31] P.F. da Silva, J.D. de Oliveira, J.B. Copetti, M.H. Macagnan, E.M. Cardoso, Flow boiling pressure drop and flow patterns of R-600a in a multiport minichannels, International Journal of Refrigeration. (2023). https://doi.org/10.1016/j.ijrefrig.2023.01.001.
[32] M. Klugmann, P. Dąbrowski, D. Mikielewicz, Flow distribution and heat transfer in minigap and minichannel heat exchangers during flow boiling, Appl Therm Eng. 181 (2020). https://doi.org/10.1016/j.applthermaleng.2020.116034.
[33] K. Strąk, M. Piasecka, B. Maciejewska, Spatial orientation as a factor in flow boiling heat transfer of cooling liquids in enhanced surface minichannels, Int J Heat Mass Transf. 117 (2018) 375–387. https://doi.org/10.1016/j.ijheatmasstransfer.2017.10.019.
[34] K. Strąk, M. Piasecka, The applicability of heat transfer correlations to flows in minichannels and new correlation for subcooled flow boiling, Int J Heat Mass Transf. 158 (2020). https://doi.org/10.1016/j.ijheatmasstransfer.2020.119933.
[35] K. Płaczkowski, M. Grabowski, M.E. Poniewski, Novel twofold use of photographic technique for simultaneous flow boiling image recording and void fraction computation in a mini-channel experiment, Energies (Basel). 14 (2021). https://doi.org/10.3390/en14154478.
[36] M. Piasecka, B. Maciejewska, A. Piasecki, Heat Transfer Calculations during Flow in Mini-Channels with Estimation of Temperature Uncertainty Measurements, Energies (Basel). 16 (2023) 1222. https://doi.org/10.3390/en16031222.

■